

Linked detachment folds, thrust faults, and salt diapirs: observations and analog models

Mark G. Rowan^{1*}, Josep Anton Muñoz², Eduard Roca², Oriol Ferrer², Pablo Santolaria², Pablo Granado², Marco Snidero²

¹ Rowan Consulting, Inc., 850 8th St., Boulder, CO 80302, USA mgrowan@frii.com
1.303.545.9437

² Institut de Recerca Geomodels, Departament de Dinàmica de la Terra i de l'Oceà, Universitat de Barcelona, Barcelona, Spain jamunoz@ub.edu eduardroca@ub.edu joferrer@ub.edu pablo.santolaria.otin@gmail.com pablomartinez_granado@ub.edu marcosnidero@gmail.com

ABSTRACT

Contractional deformation in salt-bearing rifted- and convergent-margin settings often involves diapirism. Diapirs may predate the onset of shortening, such that they exert a pronounced influence on how contractional strain is accommodated, or they may be triggered by the shortening. Analog models have been used to help understand the interaction and evolution of detachment folds, thrust faults, and diapirs, but few surface or subsurface datasets provide adequate three-dimensional images to test and refine the experimental results. Here we use 3D depth-migrated seismic data from the Sureste Basin, offshore SE Mexico, to map two structures, one dominated by salt-cored anticlines and one characterized by thrust faults. Associated diapirs include both pre- and syncontractional stocks and walls. We show that although analog models in the literature nicely reproduce some of the seismic geometries, there are also apparent mismatches. Whereas models often generate decapitated diapirs and thrust-fault salients centered on the diapirs, such features are absent in the study area. Moreover, in contrast to model thrust faults that dip 20-45°, faults in the study area are steeper, ranging from 50-75°. We bring in observations from other salt basins to discuss these discrepancies, possible explanations, and suggestions for improving the applicability of models to nature.

Keywords: Detachment folds, thrust faults, salt diapirs, analog models, Gulf of Mexico

1. Introduction

The presence of salt exerts a profound influence on contractional deformation because of its ductile rather than brittle nature. Shortening detached on salt is characterized by broad belts with narrow cross-sectional taper, an overall symmetric deformation style, elongate salt-cored anticlines and broad synclines, and map-view patterns controlled by the areal distribution and thickness of the salt layer (Davis and Engelder, 1985). Examples are known from numerous convergent- and divergent-margin fold-and-thrust belts and the styles have been replicated in analog models (Costa and Vendeville, 2002; Smit et al., 2003; and many others).

Salt diapirs can be triggered during contraction, either from the cores of detachment folds (Coward and Stewart, 1995) or from salt carried up in the hanging walls of thrust faults

emanating from the salt layer (e.g., Hudec and Jackson, 2006). If the overburden is thick, syntectonic erosion plus/minus crestal extensional faults are required to thin the roof enough for salt to break through and begin diapirism. Examples are known from such varied provinces as the southern Pyrenean foreland, the Central North Sea, and the southern Gulf of Mexico (e.g., Sans and Koyi, 2001; Karlo et al., 2014; Rowan, 2019), but relatively few analog models have progressed to the point of salt breakout and subsequent diapirism (Table 1 and references therein; Fig. 1A).

The geometries become more complex when there are established salt diapirs that predate the shortening. This scenario is common in numerous convergent-margin fold-and-thrust belts including the Pyrenees and Prebetics of Spain, the French and Austrian Alps, the Atlas Mountains, the Zagros Mountains, and the Flinders Ranges of Australia (e.g., Letouzey and Sherkati, 2004; Roca et al., 2006; Rowan and Vendeville, 2006; Saura et al., 2014; Cámara, 2017; Granado et al., 2018; Célini et al., 2020). It is also typical of deepwater foldbelts on salt-bearing rifted margins such as the northern and southern Gulf of Mexico and the Lower Congo Basin of West Africa (e.g., Rowan et al., 2000; Gottschalk et al., 2004; Davison et al., 2020). The presence of preexisting diapirs strongly influences the structural style because the weak diapirs tend to localize contractional strain (Vendeville and Nilsen, 1995), with salt-cored detachment folds and thrust faults typically extending away from, and connecting, the diapirs (e.g., Rowan and Vendeville, 2006; Callot et al., 2007).

Abundant research has examined the effects of preexisting diapirs on contraction using analog (sandbox) models (Table 1 and references therein). Setups have ranged from single diapirs to various arrangements of multiple diapirs, with some models having diapirs that were triggered by differential loading or extension and other models using pre-constructed diapirs. Moreover, many variables have been examined, including the plan-view shape (stock or wall – axial ratio of

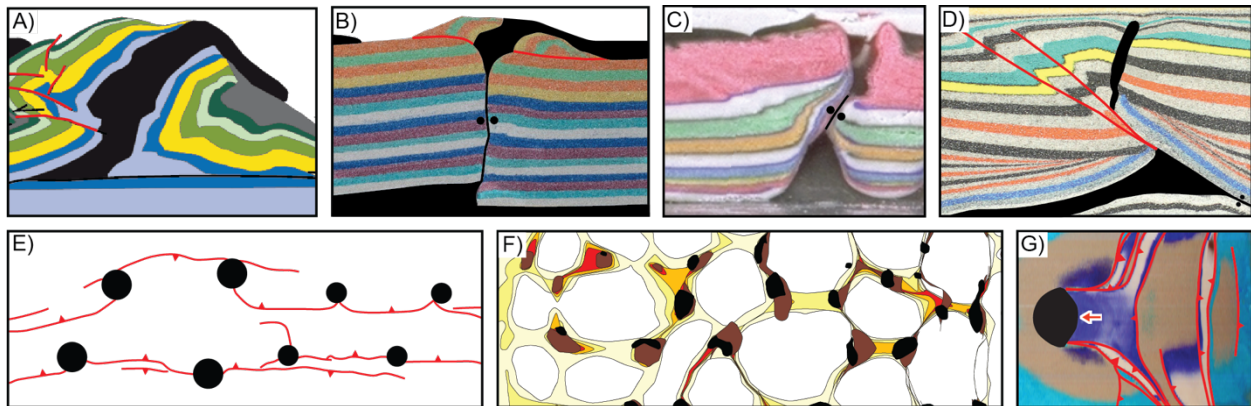


Fig 1. Published analog models of diapirs and contractional structures (salt analog in black, thrust faults in red, welds with pairs of dots; no scales shown). Cross-sectional views: (A) salt sheet breaking out from eroded crest of isoclinal salt-cored anticline (modified from Santolaria et al., 2015); (B) vertical weld due to squeezing of a constructed preexisting diapir (modified from Duffy et al., 2018); (C) steep thrust weld (remnant of preexisting diapir created by differential loading) with equally steep hanging-wall strata (modified from Rowan and Vendeville, 2006); (D) decapitated preexisting diapir due to offset on thrust fault emanating from apex of pedestal (modified from Roma et al., 2018). Map views: (E) broadly linear pattern of thrust faults linking preexisting diapirs, with common local curvature into the salt (modified from Callot et al., 2007); (F) polygonal pattern of squeezed preexisting diapirs linked by contractional structures rooted in deep preexisting salt ridges shown by non-black colors (modified from Rowan and Vendeville, 2006); (G) indenter (red arrow) in hanging wall of thrust faults that curve toward a preexisting diapir, forming a thrust salient (modified from Dooley et al., 2015, major thrust faults with larger red triangles).

Table 1. Published analog models of shortening-related diapirs.

Publication	Pre-shortening configuration					Cross-section (final)		Final map pattern
	Initiation	Diapirs	Roof	Pedestal	Source	Diapirs	Thrusts	
Sans & Koyi 2001	no diapirs					vertical, open	folds	?
Costa & Vendeville 2002	no diapirs					vertical, open	25-45°	linear
Bonini 2003	no diapirs					inclined, open	?	?
Brun and Fort 2004	no diapirs					vertical/inclined, open to welded	25-45°	?
Santolaria et al. 2015	no diapirs					vertical, open	20-40°	linear
Borderie et al. 2018	no diapirs					vertical, open	20-30°	linear
Pla et al. 2019	no diapirs					vertical, open	folds	linear
Nilsen et al. 1995	differential loading	vertical stocks & walls	thick	small	welded	vertical, open	35°	arcuate
Letouzey et al. 1995	prebuilt	vertical, short	thick	none	open	vertical to inclined, open	30-45°	?
Koyi 1998	differential loading	vertical	none	?	?	vertical to inclined	?	?
Guglielmo et al. 2000	extension	vertical wall	none?	large	?	50-90° welds	faulted folds	linear
Letouzey & Sherkati 2004	prebuilt	vertical stocks	thin	large	open	open to 50-90° welds	30-45°	curvature into diapirs
Roca et al. 2006	extension	vertical walls	none	large	open	50-90° welds, decapitation	folds, steep thrusts	arcuate
Rowan & Vendeville 2006	differential loading	vertical stocks	thick	large	welded	open to 65-90° welds	30-45°	polygonal
Callot et al. 2007	prebuilt	vertical stocks	thin & thick	none	open	40-90° welds, decapitation	20-45°	curvature into diapirs
Dooley et al. 2009a	prebuilt	vertical walls	thick	none	open	70-90° welds, decapitation	25-45°	arcuate
Dooley et al. 2009b	prebuilt	single inclined stock	thick	small	open	inclined open to welded	35-40°	arcuate, indenters
Callot et al. 2012	prebuilt	vertical stocks & walls	thin & thick	small to none	open to welded	60-90° welds, decapitation	folds	arcuate
Ferrer 2012	differential loading	vertical stocks and walls	thin	large	welded	vertical welds, decapitation	folds, 30-40° thrusts	curvature into salt, arcuate
Dooley et al. 2015	prebuilt	one vertical or inclined stock	thin & thick	none	open	65° weld	moderate-dip thrusts	curve into salt, indenters
Duffy et al. 2018	prebuilt	vert & inclined stocks & walls	thin & thick	none	open	vertical & thrust welds, decap.	30°	curve into salt, indenters
Roma et al. 2018	extension	vertical walls	none	large	open to welded	vertical welds, decapitation	30-40°	curvature into diapirs
Dooley & Hudec 2020	extension	vertical walls	thin	large	open to welded	45-90° welds	folds, 30-40° thrusts	arcuate
Santolaria et al. 2021a	prebuilt	vertical & inclined walls	thin & thick	small to none	welded	65-90° welds, decapitation	25-30°	curve into salt, indenters
Santolaria et al. 2021b	differential loading	vertical stocks & walls	none/thick	large	welded	70-90° welds, decapitation	25-35°	polygonal, indenters
Sebai et al. 2021	prebuilt, extension	vertical walls	thick	none	welded	open, vertical welds	25-35°	linear

<2 or >2, respectively), the cross-sectional geometry (vertical or inclined), the presence and geometry of diapir pedestals, the orientation relative to shortening, the thickness of the salt layer (including whether or not it has been evacuated to form a salt weld), the thickness of the diapir roof, the sedimentation/erosion, and the deformation rate. Typical salt features observed in model cross sections include vertical salt welds, inclined thrust welds, decapitated diapirs, and

flaring or allochthonous salt (Fig. 1B-D). Map patterns range from linear or arcuate to polygonal (Fig. 1E-F). Thrust faults that typically dip 25-45° tend to curve toward the diapirs, with sharp curvature on both sides of a diapir creating thrust-fault salients or reentrants that have been termed indenters if the diapir is located toward the foreland relative to the deeper part of the thrust fault (Fig. 1G).

In this short paper, we use 3-D, depth-migrated seismic data from the Sureste Basin in the southern Gulf of Mexico to examine the usefulness and limitations of analog models in understanding the interaction between diapirs, detachment folds, and thrust faults. Note that we deal primarily with passive diapirs (ones that grow at or just beneath the surface as sediment is deposited; Rowan and Giles, 2021), whether in the form of salt stocks, salt walls, or salt sheets. Moreover, we focus on so-called isolated-diapir provinces (i.e., diapirs largely surrounded by minibasin strata) rather than isolated-minibasin provinces (Duffy et al., 2017). In contractional systems involving isolated diapirs, one of the key questions is how much analog models can be relied upon to help determine whether diapirs predated the shortening or were triggered by the shortening. We suggest that the answer is not always clear-cut but that model results provide a useful tool that should be employed. We start by summarizing the tectonic and structural evolution of the Sureste Basin and then briefly describing the three-dimensional geometries of two specific elongate structures with multiple diapirs. We then evaluate the observed relationships in light of both published and unpublished analog models, not just of the study area but also of other salt-bearing contractional provinces, and suggest possible ways of moving forward to improved matches between models and nature.

2. Sureste Basin, southern Gulf of Mexico

2.1. Geologic setting and dataset

The Sureste Basin is unusual in that it is both a divergent margin and part of a convergent margin, having experienced both gravity-driven and orogenic deformation. The history below is summarized from Sánchez-Rivera et al. (2013), Rowan (2019), and Davison (2020). The Middle Jurassic salt was deposited late in the rift history, just prior to the onset of oceanic spreading. Postsalt deformation can be divided into three overlapping phases (Fig. 2). First, Late Jurassic to Cretaceous gravity gliding was caused by differential thermal subsidence and consequent basinward tilting of the margin. The arcuate shape of the margin resulted in convergent, W- to N-directed movement. Second, the Mexican and Chiapaneco orogenies caused Paleogene to middle Miocene, somewhat arcuate, NE-directed shortening. Third, sediment shed from the Chiapas Massif loaded the margin and caused late Miocene to Recent, slightly divergent, NNW-directed gravity spreading. Structural orientations thus varied both spatially and temporally and there was significant overprinting of earlier structures. In addition to the basal salt detachment, weak Paleogene shales provided a secondary detachment that resulted in partly decoupled deformation in places.

The study area, located in the deepwater province of the Bay of Campeche, is approximately 200-250 km from the coastline and 50-100 km from the western edge of the salt basin (Figs. 2, 3 inset). It is covered by a wide-azimuth (WAZ), RTM depth-migrated, 3-D seismic volume from Schlumberger, and the nearest well control is roughly 75 km away.

Aside from salt features and faults, two main horizons were interpreted in three dimensions on each structure (deep and shallow). The ages of the horizons are not specified due to

confidentiality, but note that the shallow horizon in the two structures is not the same age. Around the study area, growth geometries indicate that there was an initial, minor phase of shortening during the Eocene (slightly younger than the deep/green horizon), at most subtle shortening during the Oligocene to early Miocene, and the main phase of shortening during the middle Miocene to present (younger than the shallow/orange horizons).

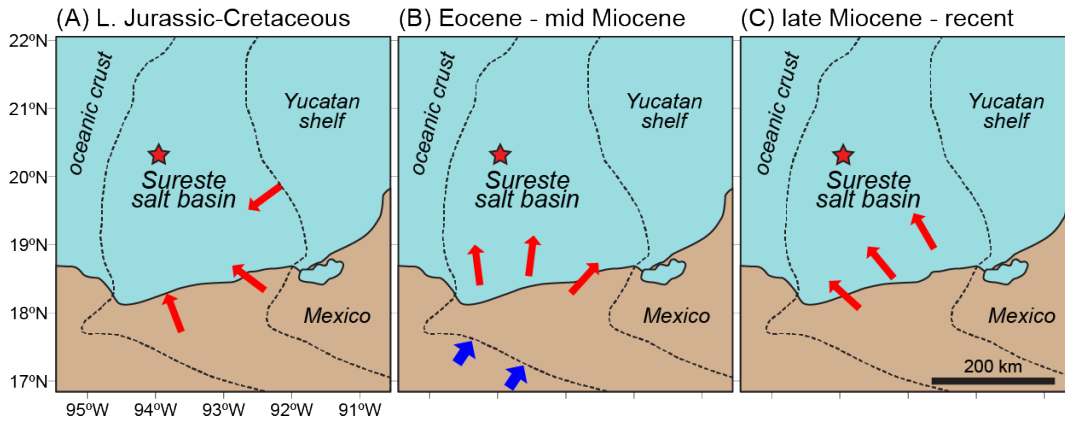


Fig. 2. Evolution of gravity-driven and orogenic deformation in the Sureste Basin (modified from Rowan, 2020, after Sánchez Rivera et al., 2021). Black dashed line outlines the salt basin (from Hudec et al., 2013); red arrows denote generalized movement directions detached on salt; blue arrows show direction of orogenic deformation; red star shows the approximate location of the study area. See text for explanation of evolution.

2.2. Structure 1

The first structure evaluated (Figs. 3, 4, S1) is a minimum of 25 km long, extending out of the data volume to the west. It comprises two diapirs along a structure that is fold-dominated at the shallow level. From SW to NE, we see: (i) three salt-detached thrust imbricates at the deep level but a decoupled shale-detached fold with minor thrust faults at the shallow level (Figs. 3A, S1A); (ii) 3.6 km away, a NW-directed thrust fault dipping $\sim 65^\circ$ and smaller backthrust at the deep level overlain by a taller, upright, almost isoclinal fold at the shallow level (Figs. 3B, S1B); (iii) 2.8 km to the NE, a narrow vertical diapir (Diapir 1-1) flanked by concordant and conformable vertical strata on both flanks and transitioning into a subhorizontal salt sheet (Figs. 3C, S1C); (iv) 3.3 km along strike, back to a 65° -dipping NW-directed thrust fault with two backthrusts at the deep level overlain by a tight fold dissected by several crestal extensional faults (Figs. 3D, S1D); (v) 3.5 km away, a relatively simple anticline with a pop-up structure at the deep level, with the NW-directed thrust fault connected between the two stratigraphic levels but distinct SE-directed thrust faults at each level (Figs. 3E, S1E); (vi) 4.8 km to the NE, a partly decoupled structure with a SE-vergent faulted fold at the deep level and a 65° -dipping NW-vergent thrust fault linked to shallow salt (Diapir 1-2) at the shallower level (Figs. 3F, S1F); and (vii) 2.3 km along strike, a lower-amplitude thrust anticline with separate thrust faults at the two levels, with the shallower thrust fault dipping $\sim 50^\circ$ (Figs. 3G, S1G). The strike line (Figs. 3X, S1X) shows two diapirs connected to the autochthonous layer, with each forming a culmination along the structure.

In plan view (Fig. 4), the diapirs are located along the fold crest, with the fold plunging away from the diapirs in both directions and an elevated saddle between the two diapirs. Thrust faults curve up to 90° to intersect the diapirs, usually at cusps in the edge of salt. Normal faults extend

away in both directions from Diapir 1-1, where there is also a prominent unconformity on the NE flank; both features are absent at Diapir 1-2. Moreover, a smaller NNW-trending structure intersects the main fold at Diapir 1-2 (Fig. 4B). Finally, elongate allochthonous sheets advanced mostly basinward (to the NW) from both diapirs.

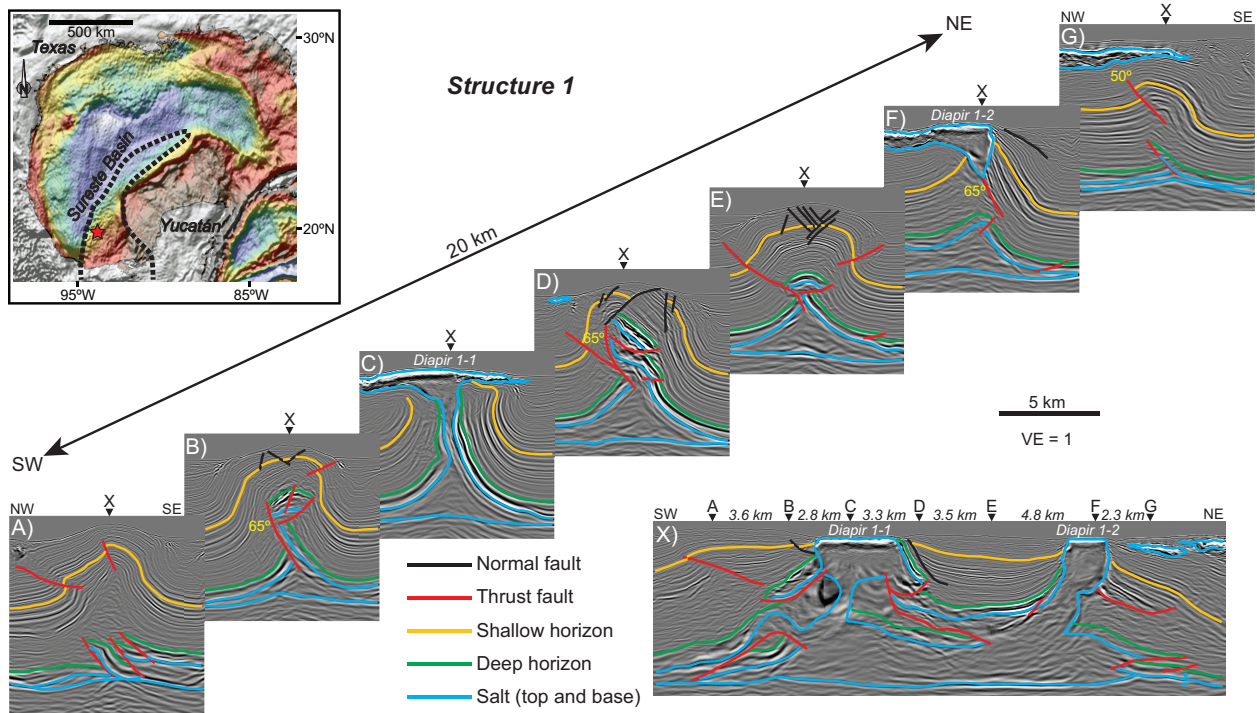


Fig. 3. Depth-migrated seismic profiles illustrating the along-strike geometry of Structure 1 (WAZ RTM data courtesy of Schlumberger): (A) to (G) – dip lines; (X) strike line. See supplementary Figure S1 for uninterpreted versions of the lines. Numbers in yellow are the average dips of significant thrust faults; pairs of blue dots denote salt welds. All lines shown with no vertical exaggeration (VE); location of lines shown in Fig. 4. Inset shows free-air gravity image of Gulf of Mexico (courtesy of N. Kuszniir) with Sureste Basin outlined in dotted line and general location of the study area indicated by the red star.

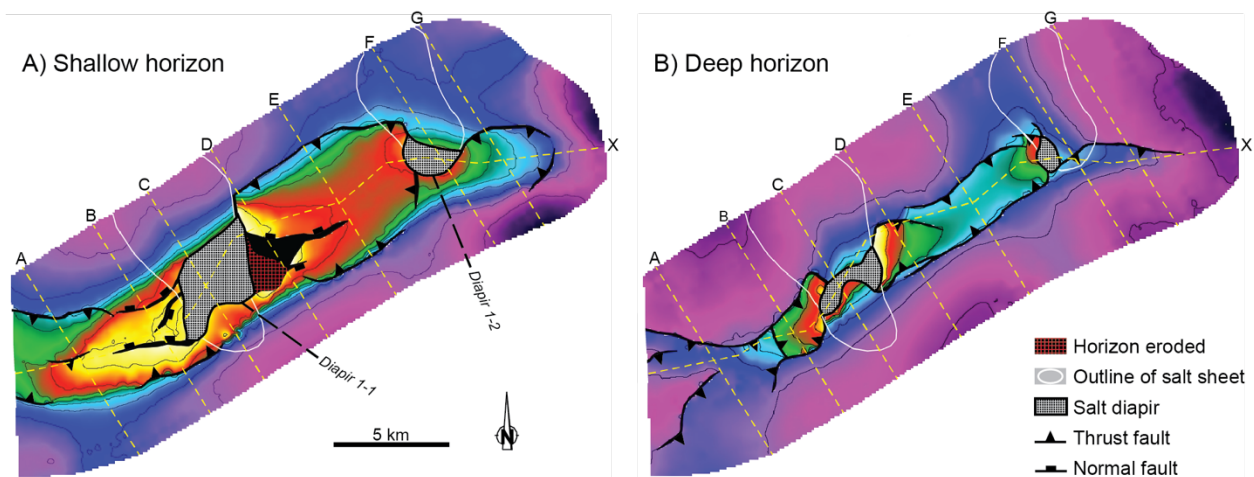


Fig. 4. Depth structure maps of Structure 1 derived from the 3D seismic data: (A) shallow horizon (orange in Fig. 3); (B) deep horizon (green in Fig. 3). No depth scale is shown, but cool colors are deeper and warm colors are shallower (contour interval is 500 m). Yellow dashed lines are the seismic profiles of Fig. 3.

2.3. Structure 2

The second structure (Figs. 5, 6, S2) is approximately 40 km long between two prominent saddles. It is dominated by steep thrust faults connecting three diapirs: a 16-km long, partially welded salt wall (Diapir 2-1) to the SW; and two smaller salt walls to the NE (Diapirs 2-2 and 2-3). From SW to NE, we see: (i) a SE-vergent, 60°-dipping thrust fault with two minor thrust faults in its footwall (Figs. 5A, S2A); (ii) 6.0 km away, a near-vertical salt weld representing the feeder to Diapir 2-1, with moderately-dipping truncated strata on both flanks (Figs. 5B, S2B); (iii) 3.0 km to the NE, a slightly inclined diapir (also part of Diapir 2-1) with truncated strata on its NW flank and concordant strata on its SE flank (Figs. 5C, S2C); (iv) 4.7 km along strike, a NW-vergent, 65°-dipping thrust fault, with several hanging-wall backthrusts and a series of shallow normal faults that truncate the oldest hanging-wall strata (Figs. 5D, S2D), that links to a steep weld and shallow salt sheet; (v) 5.6 km away, a 75°-dipping thrust fault, with several rotated imbricate backthrusts in the hanging wall and a truncated anticline in the footwall, carrying salt to levels just beneath crestal normal faults (Figs. 5E, S2E); (vi) 3.2 km to the NE, an inclined diapir (Diapir 2-2) with a similar stratal geometry but with a lower SE flank and no anticline on the NW flank (Figs. 5F, S2F); and (vii) 7.3 km along strike, a NW-vergent, 70°-dipping thrust fault with crestal normal faults and opposite-vergence thrust faults in its footwall (Figs. 5G, S2G). The strike line (Figs. 5Y, S2Y) shows a major culmination near the intersection with Line A, a minor culmination near the center of Diapir 2-1, and a broad culmination near Lines E and F that is dissected by numerous crestal normal faults. Local shifting depocenters are indicated by white lines on Fig. 5Z.

In plan view (Fig. 6), Structure 2 is linear except along Diapir 2-1, which has a sigmoidal shape between its SE-vergent SW half and its NW-vergent NE half. Four structural highs intersect at Diapir 2-1: the WNW-plunging termination of Structure 2; a thrust anticline extending to the SW; a subtle ridge trending SE roughly along the trace of Line 5B; and the thrust fault that links Diapirs 2-1 and 2-2. Similarly, three structural highs intersect at Diapir 2-3: the ENE-plunging termination of Structure 2; a N-S trending thrust anticline that continues out of the data to the N; and the thrust fault linking Diapirs 2-2 and 2-3. Unlike in Structure 1, the thrust faults exhibit little to no curvature approaching the diapirs, and they intersect the pointed terminations of the diapirs instead of cusps in the salt edge. Crestal normal faults are well developed from approximately the middle of Diapir 2-1 to Diapir 2-2. Finally, Diapirs 2-2 and 2-3 fed small salt sheets that advanced basinward (to the NW); in contrast, whereas the NE half of Diapir 2-1 also sourced a salt sheet that advanced basinward, the SW half fed a sheet that advanced landward (to the SE).

3. Discussion

The three-dimensional interaction between detachment folds, thrust faults, and diapirs in Structures 1 and 2 are exceptionally well constrained due to the high-quality new WAZ images. Nevertheless, a key question is whether the diapirs predated the shortening or broke out during the contractional deformation. In other words, did preexisting diapirs influence how contractional strain was subsequently accommodated, or did shortening of a thick overburden eventually lead to salt breakout and consequent diapirism? In the sections below, we first use seismic observations and analog models to answer the question, and then use geometries from

the Sureste Basin and other salt basins to discuss the general applicability and limitations of experimental models in understanding salt-detached contractional deformation.

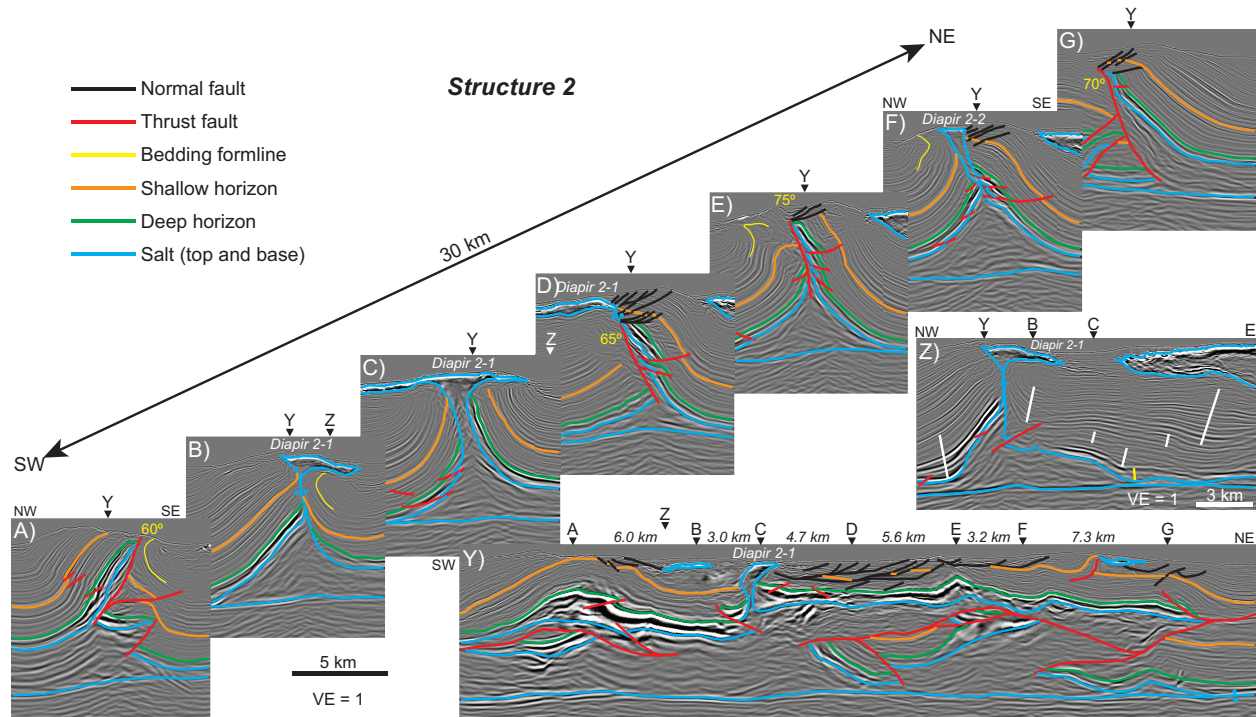


Fig. 5. Depth-migrated seismic profiles illustrating the along-strike geometry of Structure 2 (WAZ RTM data courtesy of Schlumberger): (A) to (G) – dip lines; (Y) strike line; (Z) oblique line (with different scale). See supplementary Figure S2 for uninterpreted versions of the lines. Numbers in yellow are the average dips of significant thrust faults; pairs of blue dots denote salt welds, white lines in (Z) indicate shifting depocenters. All lines except (Z) shown with no vertical exaggeration (VE); location of lines shown in Fig. 6.

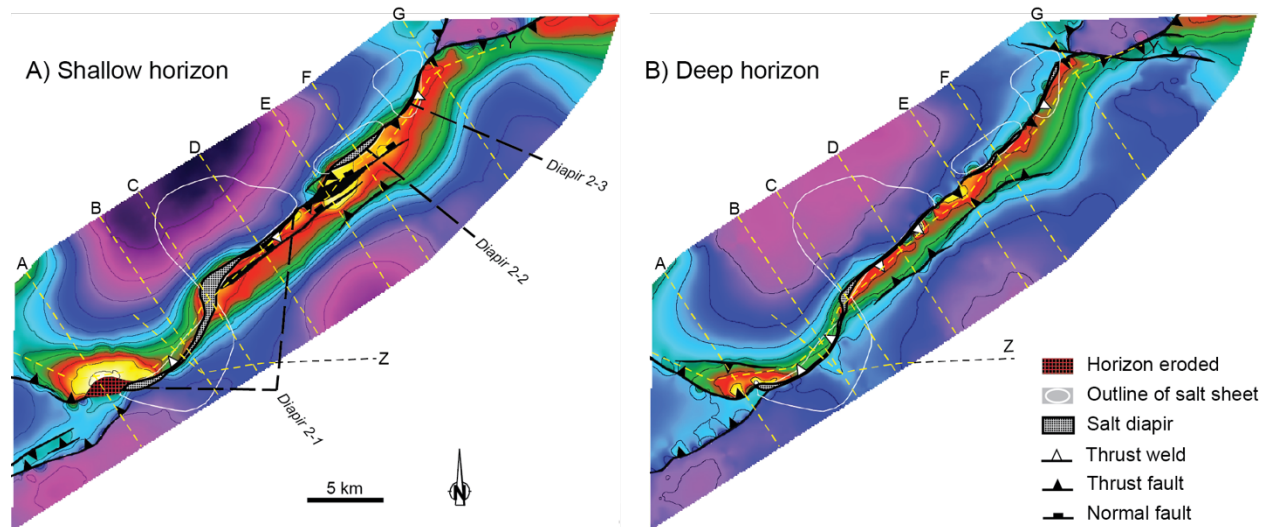


Fig. 5. Depth structure maps of Structure 2 derived from the 3D seismic data: (A) shallow horizon (orange in Fig. 5, not the same age as the orange horizon in Fig. 3); (B) deep horizon (green in Fig. 5). No depth scale is shown, but cool colors are deeper and warm colors are shallower (contour interval is 500 m). Yellow dashed lines are the seismic profiles of Fig. 5.

3.1. Early vs late diapirs

The most conclusive evidence for preexisting diapirs is the presence of features that formed during passive diapirism in strata older than the onset of shortening. Such features take the form of near-diapir halokinetic sequences, local angular unconformities, and reworked diapir- or roof-derived detritus in flanking sediments (e.g., Giles and Lawton, 2002; Rowan et al., 2003; Giles and Rowan, 2012). Whereas this evidence is common around exposed diapirs, it is more rarely documented by well data or visible on seismic data (e.g., Hearon et al., 2014; Pichel and Jackson, 2020).

In the absence of observed halokinetic sequences, larger-scale stratal geometries can provide clues. Salt rising in passive diapirs flows from beneath subsiding minibasins. These commonly display multiple-km scale wedge-shaped minibasin tectonostratigraphic successions (Rowan and Giles, 2021) that record the subsidence history and salt-flow kinematics. However, models suggest that differential loading does not always result in minibasin thickness changes (e.g., Nilsen et al., 1995; Koyi, 1998; Rowan and Vendeville, 2006). Moreover, the geometries can be subtle in contractional settings as even small amounts of shortening can drive ongoing passive diapirism (Vendeville and Nilsen, 1995). In the case of Structures 1 and 2, a first glance reveals at best minor evidence of salt evacuation prior to the main shortening event in most locations (Figs. 3, 5), but again, this is inconclusive. More importantly, Diapir 1-2 has thin strata on one flank and thickened strata on the other, only part of which is structural (Fig. 3X), and strata on the SE flank of Diapir 2-1 (Fig. 5B) are anomalously thin. More convincing is an oblique line through the SW part of Diapir 2-1 with obvious salt-evacuation geometries (white lines, Fig. 5Z).

Using analog models is helpful but often provides non-unique answers. For example, linear map patterns can be associated with both pre- and syncontractional diapirs (Table 1). Moreover, although there are many models of preexisting diapirs, relatively few exist that examine late breakout of salt (Table 1). Model shortening of established diapirs generates such structures as steep welds, diapir decapitation, and thrust salients and reentrants (Fig. 1B-G). But what are the characteristic styles when diapirism is syncontractional? One consistent feature is that the oldest minibasin strata come up to a very shallow level on at least one diapir flank, if not both (Figs. 1A, 7A). However, this geometry is not diagnostic, as steep and shallow panels of suprasalt strata can also represent non-contractional, halokinetic megaflaps (Rowan et al., 2016). Another characteristic style of late breakout is that any thick prekinematic stratigraphic section is thinned by some combination of erosion and/or crestal normal faults (Fig. 7A), which is related to the inability of salt to break through a thick overburden (e.g., Vendeville and Jackson, 1992, and many others). In plan view, the diapirs and associated folds or thrust faults tend to be linear (Fig. 7B).

We use a combination of seismic observations and analog model results to argue that there is a mixture of preexisting diapirs and late, syncontractional diapirs along Structures 1 and 2.

Diapir 1-1. This is most likely a late diapir. The deepest strata come all the way up both flanks, there is significant erosion, and crestal normal faults are abundant (Figs. 3C-D and X, 4A, S1C-D). There is thinning between the deep and shallow horizons just to the SW of the diapir (Figs. 3C, X, S1C) that might suggest early diapirism, but this is interpreted as thinning due to either an Eocene phase of thrusting or ductile flow of Eocene shales during late decoupled shortening.

Diapir 1-2. This is interpreted as a preexisting diapir. There are significant thickness variations in precontractional strata, the diapir is at the intersection of three structural highs,

the oldest strata are at depth except for very locally on its NW flank, and shallow normal faulting and erosion are minimal (Figs. 3F and X, 4A-B, S1F).

Diapir 2-1. This salt wall is interpreted as a combination. The SW half is a preexisting diapir, with prominent minibasin growth geometries, a location at the intersection of four structural highs, a vertical weld with truncation of the oldest strata at depth, and minimal shallow extension (Figs. 5B, Y, Z, S2B, Y, Z). In contrast, the NE half likely represents late breakout of salt, as suggested by the shallow oldest strata on its SE flank and abundant crestal faulting (Figs. 5C-D and Y, 6A, S2C-D and Y). Each half generated its own salt sheet, with lateral flow in opposite directions, probably driven by the opposing-vergence thrust faults.

Diapir 2-2. This diapir is more enigmatic. Stratal thickness changes are minor and there are crestal normal faults, especially to the SW (Figs. 5E-F, 6A, S2E-F), so it might appear to be late. However, the oldest strata still have about 1 km of overburden at their shallowest point (Figs. 5E, S2E), making it mechanically unlikely for the salt to have broken through, and thus probably an early rather than late diapir. Interestingly, the oldest strata are shallowest not at the diapir but slightly to the SW (Fig. 6B), with prominent normal faults and erosion just above, and yet the salt did not break through in this location (Fig. 5E, S2E).

Diapir 2-3. This diapir, not illustrated here in cross-sectional view, is also enigmatic. Most of it is a vertical weld with 1-2 km of overburden above the oldest strata, and it's located at an intersection of three structural highs (Fig. 6). But evidence of precontractional salt evacuation is absent, and the oldest strata do get very close to the base of the shallow salt at its eastern end (Figs. 5G, S2G). The origin of the diapir is therefore uncertain.

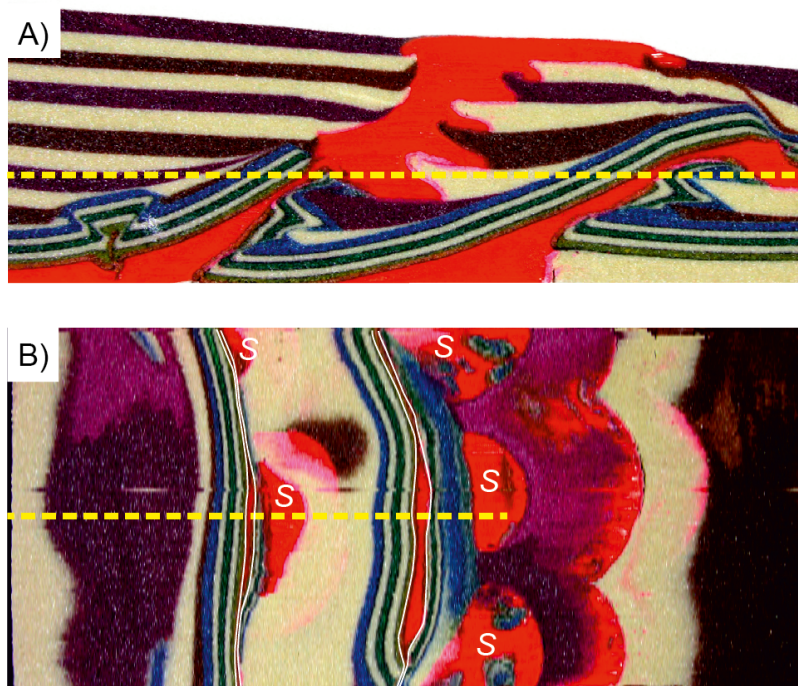


Fig. 7. Section of an analog model at the end of the experiment showing late breakout of salt (scales not shown): (A) salt (red) breaking out from hanging wall of source-fed thrust and rising passively during ongoing deposition (yellow line is depth slice of B); (B) depth slice of the same experiment (level shown in A) illustrating linear system of salt walls and thrust welds (outlined in white), and local allochthonous sheets (in red with white letter S; not to same scale as A).

One possibility that must be considered is that each structure originated as a salt wall along its entire length, but that some portions grew higher than others prior to shortening. However, we see no evidence for this in the observed geometries of the deeper thrust-dominated structures or in the minibasin thickness patterns. Instead, it is more likely that there was a series of Eocene contractional structures, some of which evolved into diapirs prior to the main phase of shortening. Testing this idea would require a full three-dimensional restoration to remove the late deformation, something beyond the scope of this work.

3.2. Comparison of analog models and natural structures

We have suggested that Structures 1 and 2 have diapirs along their trends that are both pre- and syncontractional. There is no single observation that allows us to determine the origins of the diapirs, nor are there any aspects of these diapirs or flanking strata that are shown by analog models to be exclusively characteristic of one origin or the other. This is not always the case: for example, decapitation has been generated only in published models with preexisting diapirs, but we observe no decapitation. In general, it is only the combination of multiple observations and model results that allow proper identification of the evolution.

There are numerous other data sets that can be used to test the models, including both outcrop and subsurface structures. Many features observed in nature are simulated nicely in the laboratory. However, in the following discussion, we use the Sureste Basin and other salt basins to examine three aspects that warrant further analysis and explanation: the prevalence of diapir decapitation in models, the nature and development of thrust salients and reentrants, and the steepness of thrust faults/welds and associated hanging-wall strata adjacent to or between diapirs.

3.2.1. Diapir decapitation

Thrust faults that decapitate welded diapirs are common in analog models (Fig. 1D, Table 1). They usually emanate from the apices of remnant pedestals but more rarely may root elsewhere and cut the diapir some distance above the pedestal. They have not been observed in the study area (or anywhere else in the Sureste Basin to our knowledge), but there are a few mentions or depictions of decapitation (or beheading) in provinces such as the Zagros Mtn. of Iran (Talbot and Alavi, 1996; Snidero et al., 2019), the northern Gulf of Mexico (Grando and McClay, 2004), the Eastern Cordillera of Colombia (Parravano et al., 2015), and the Southern Carpathians of Romania (Tămaş et al., 2021). However, these are very much the exception in the literature and in our examination of seismic and outcrop data from various basins.

Why is decapitation apparently rare in nature but more common in models? First, it may be related to the suitability of model materials for mimicking nature, for example because of the low cohesion of sand used to represent sedimentary overburden. On the other hand, decapitation may actually be more prevalent in the subsurface of exposed orogenic belts, especially if thrust nappes cut across diapirs rooted in salt more toward the foreland (e.g., Tămaş et al., 2021), but difficult imaging has inhibited its interpretation. Deepwater contractional provinces, however, are much better imaged and decapitated diapirs are largely absent. One possible explanation is the amount of shortening, since decapitation typically occurs only after a secondary weld has formed. Gravity-driven shortening is usually of low magnitude compared to that in orogenic belts (e.g., Rowan et al., 2004). More importantly, whereas the total shortening in nature is usually distributed across many diapirs and associated thrust faults, often over long distances, any given diapir may not experience enough deformation to lead to decapitation. In contrast, the

total contractional strain in analog models is accommodated by just one or a few diapirs, leading to post-welding ongoing thrusting and thus decapitation.

3.2.2. *Thrust salients and reentrants*

The term indenter, first used by Dooley et al. (2009b) and adopted by others in describing model geometries (Table 1), has been applied to structures bounded by strike-slip or oblique-slip cross faults on the hinterland/landward sides of diapirs, whether in a thrust hanging wall (Fig. 1G) or a thrust footwall (e.g., Dooley et al., 2015; Duffy et al., 2018). Here, however, we refer to them as thrust salients and reentrants, respectively. The terms are used in the local sense of an individual thrust fault, whether foreland-vergent or a backthrust, rather than the regional sense of an entire fold-and-thrust belt.

Although both salients and reentrants have been generated in analog models, our study area contains only minor reentrants at the shallow level of Diapir 1-2 (Fig. 4A) and the deep level of Diapir 1-1 (Fig. 4B). Crucially, the former is interpreted as a preexisting diapir and the latter as a late diapir, suggesting that fault curvature cannot be used to distinguish between pre- and syncontractional diapirs. Both are along Structure 1, which is dominated at the shallow level by detachment folds with minor, relatively low-angle thrust faults cutting the limbs (Fig. 3). In contrast, there are no reentrants along the length of Structure 2 (Fig. 6), which is dominated at all levels by steep thrust faults (Fig. 5). Thrust reentrants centered on squeezed diapirs have also been illustrated from other deepwater provinces such as the Lower Congo Basin (Jackson et al., 2008) and the northern Gulf of Mexico (Rowan and Ratliff, 2012). We are unaware, however, of documented thrust salients at individual diapirs as produced in models (e.g., Fig. 1G). There may, however, be apparent salients due to: (i) different structural trends created by a polygonal pattern of preexisting diapirs, ridges, and minibasins; or (ii) the spacing of preexisting diapirs relative to the dominant fold/thrust wavelength controlled primarily by the thickness of the overburden. An example of the former is the apparent subtle salient along the SW half of Diapir 2-1, which is a function of the structure curving to the NW to intersect another contractional structure (NW corner of Figs. 6A and 6B).

What controls the development of thrust salients/reentrants (ignoring outcrop map patterns created by the intersection with topography)? Although there are other possible factors, the primary factor is the along-strike interaction between shortening accommodated by squeezing of a vertical diapir and that accommodated on a dipping thrust fault (Fig. 8A). If the thrust emanates from the salt layer directly along strike from the diapir, it will line up with the diapir in plan view at deep levels (red in Fig. 8B, D); at shallower levels, the trace of the thrust will curve to intersect the diapir, thereby forming a reentrant (green in Fig. 8B, C). The amount of curvature will increase going up-section or with decreased fault dip. The thrust fault will also curve more sharply where it intersects halokinetic drape folds flanking the diapir, and the detailed geometry will depend on the specific shape of the pedestal and diapir.

Why are diapirs that form localized thrust salients observed in models but apparently rare in nature? In the models where they were generated, the diapirs were prebuilt with no/little pedestals and no deep ridges of salt away from the diapirs (Table 1). In nature, there is usually a linear or polygonal pattern of deep ridges between minibasins, with the diapirs located along or at the intersections of these ridges (e.g., Rowan and Vendeville, 2006; Mount et al., 2007). As the diapirs get squeezed, folds and thrust faults nucleate along the ridges. Thus, only reentrants form if there is a linear array of ridges (Fig. 8B), but the geometries are more complex if there is a polygonal pattern. In this case, there may be apparent salients, but these are just intersections

between two thrust faults with different trends and, in fact, reentrants are still predominant (e.g., Santolaria et al., 2021b).

Another factor in the apparent scarcity of thrust salients in nature may be related to the amount, distribution, and timing of deformation. In models that resulted in thrust salients (indenters), shortening propagated away from the moving end wall so that a more hindward thrust curved sharply to intersect a weak diapir in a more forward area of the model that has experienced only layer-parallel shortening. Moreover, as mentioned before, models have only one or few diapirs, so that each diapir tends to experience more shortening, and increased shortening leads to the indenter becoming a reentrant (Dooley et al., 2015). In nature, however, shortening detached on salt may occur more or less simultaneously over large areas with many diapirs (supported by other models such as Costa and Vendeville, 2002), so that each is squeezed and develops its own associated fold or thrust without the formation of local thrust salients.

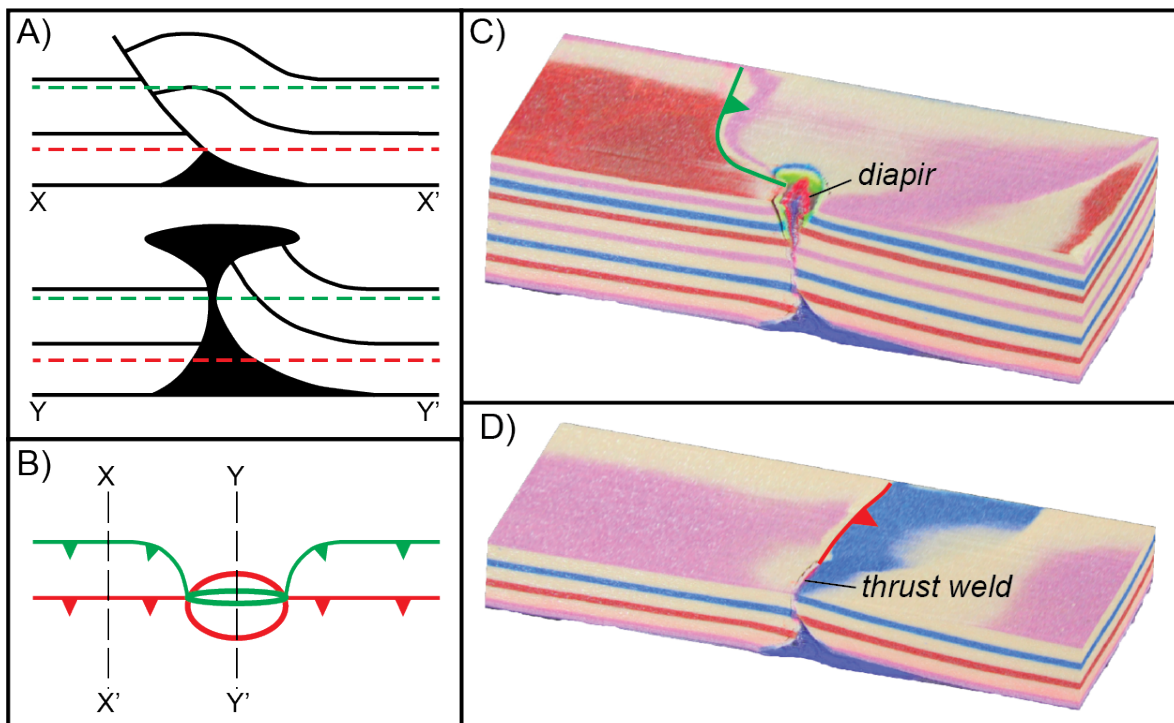


Fig. 8. Thrust salients and reentrants. (A) Schematic cross sections through thrust fault (X-X') rooted directly along strike from a squeezed preexisting diapir (Y-Y'; no salt evacuation geometries shown for simplicity); red and green dashed lines are the depths of the plan-view geometries in (B). (B) Schematic map representations of the diapir (ellipses) and thrust faults (barbed lines) at the two levels indicated in (A), with locations of the cross sections shown. (C) and (D) Depth slices of a 3D voxel image of a model showing a squeezed diapir and associated thrust fault that emanated from the salt level hindward of the diapir (analog model from Santolaria et al., 2021a, with moving end wall on the right); the model has a mirror-image geometry on the other side of the diapir that has been removed, so that from top to bottom, the thrust pattern changes from a shallow reentrant (C) to a linear trace (D).

3.2.3. Thrust-fault dip

Published model thrust faults above salt detachments have dips that span 20-45° (Table 1). Interestingly, there is no apparent correlation between fault dip and whether or not the salt layer became welded prior to the onset of shortening, despite critical-taper theory suggesting that welded salt, which is more frictional, should be associated with lower-angle thrust faults (Davis

and Engelder, 1985). In contrast to the models, major thrust faults detached at the deep salt in the study area have dips in the range of 60-75° (Fig. 5). Moreover, the attitudes are similar regardless of whether they are connected to preexisting diapirs or late diapirs. The Sureste Basin is not unique – for example, thrust faults on depth-converted seismic data from the northern Gulf of Mexico and Lower Congo Basin have dips up to 60-65° (Grando and McClay, 2004; Jackson et al., 2008). The lack of good subsurface images makes determining the dips in exposed fold-and-thrust belts difficult, but cross sections derived primarily from surface relationships in the Zagros Mts. show dips up to 65-70° (Jahani et al., 2009; Hassanpour et al., 2018). A better analog might be the Flinders Ranges of South Australia, where hanging wall strata dip very steeply and thus constrain thrust faults connecting diapirs to dips attaining 75° or even more (Vidal-Royo et al., 2021).

A related issue concerns the attitudes of strata in the hanging walls of thrust faults and thrust welds. In analog models, especially those with prebuilt diapirs and minibasins, they typically have only low to moderate dips (although there are exceptions, e.g., Fig. 1C). In nature, however, they are often sub-parallel to the steep faults/welds. This is observed in the Sureste Basin (e.g., Fig. 5) but is also characteristic of other contractional salt basins (e.g., Granado et al., 2018; Célini et al., 2020; Vidal-Royo et al., 2021).

Once again, we ask why there is an apparent mismatch between the dip of model thrust faults and associated strata and at least some of those in nature. One factor is the low cohesion of sand used in the experiments, which makes steep strata difficult to attain. Having said that, an unpublished model with very rapid synkinematic sedimentation resulted in a near vertical fault and equally steep hanging-wall strata. Another possibility is that natural thrust faults with originally low dips may steepen due to ongoing deformation such as: (i) footwall imbrication and back-rotation of an earlier thrust, as in imbricate fans; (ii) penetrative strain that steepens both strata and faults; (iii) differential evacuation of underlying salt; or (iv) progressive tightening of the shallow folds that steepens both the hanging- and footwalls as well as the faults as the salt gets squeezed. The low cohesion of sand in models, however, leads to faulting dominating over folding, such that steepening of faults during ongoing deformation is difficult to reproduce. Moreover, while modification of early low-angle thrust faults might apply in some natural cases, we have examples from the Sureste Basin where the footwall is undeformed and overlying growth strata document no rotation or folding, and yet the thrust faults still have steep dips. It may be that shortening is accommodated in a manner analogous to salt-detached normal faults that initiate as steep, planar faults over thick salt but evolve into listric shapes as the salt thins (Brun and Mauduit, 2008). In other words, early thrust faults might be relatively steep, with the hanging wall popping up on a planar fault, before the hanging-wall strata start to steepen and fold as the underlying salt thins during ongoing deformation. However, theory suggests that it is unlikely for initially steep faults to develop in natural frictional rheologies. Whatever the explanation(s) for steep thrust faults, preexisting diapirs presumably play a key role since we have observed that fault dip tends to decrease away from the diapirs.

4. Concluding remarks

The three-dimensional interaction between detachment folds, thrust faults, and diapirs, both along strike and at all structural levels, is highly complex. However, it is often uncertain due to limitations in subsurface imaging or the limited outcrop in surface exposures. Moreover, typical guidelines used for drawing cross sections in fold-and-thrust belts fail when weak diapirs and

variably-shaped minibasins predated the onset of shortening. Thus, analog models are useful tools that help us understand and predict how the geometries change along strike and with depth, whether or not diapirs were already established or formed during contraction, and how the structures initiated and evolved over time. The danger, however, is that model results may be over-applied (see Butler et al., 2020, for a discussion). For example, because only models with preexisting diapirs have generated salients/reentrants, the absence of such features might mistakenly be used to interpret that observed diapirs are syncontractional. We have shown that both early and late diapirs can have reentrants (Diapirs 1-2 and 1-1, respectively, Fig. 4) or have none (diapirs along Structure 2, Fig. 6).

Using excellent 3D seismic images from the Sureste Basin, Mexico, supported by observations from other salt basins, we have shown that analog models successfully mimic many of the structural styles found in nature. However, there are some apparent mismatches: models generate diapir decapitation and thrust salients that are rarely observed/depicted in salt basins; or models usually fail to reproduce steep thrust faults/welds and associated steep hanging-wall strata. It is possible, of course, that the model styles are much more prevalent but under-recognized in nature. Alternatively, some aspects of models may not be truly representative of most real scenarios. We suspect that both explanations are true to some extent, and thus suggest that further investigation follow two main lines of approach that should ideally be integrated. First, more detailed examples of the complex three-dimensional interactions, such as those presented here, are needed to provide more high-quality tests of model results. Second, models of these interactions need to be run with the most realistic initial configurations and physical analogs possible. In other words, models with prebuilt diapirs lacking pedestals and with mostly undeformed minibasins, although useful in a limited fashion, may be misleading. Instead, preexisting diapirs should have realistic pedestal geometries, preexisting minibasins should have synclinal strata that thin and turn up toward the diapirs prior to shortening (although other configurations also exist in nature), and comparative models should also be considered where clay is mixed into the sand to give it more cohesion and thus strength. Some existing models are already closer to real scenarios, but more are needed.

Acknowledgements

First and foremost, Schlumberger are thanked for providing MR with access to their seismic data and granting permission to show some profiles here. Partial funding for MR is through the Salt-Sediment Interaction Research Consortium at The University of Texas at El Paso, whose current sponsors are BHP, Chevron, ConocoPhillips, ExxonMobil, Hess, PGS, and Total. This work has been supported by the “Structure and deformation of salt-bearing rifted margins” project (SABREM - PID2020-117598GB-I00) funded by MCIN/AEI/10.13039/501100011033 FEDER “*Una manera de hacer Europa*”. The GEOMODELS Research Institute and the Grup de Geodinàmica i Anàlisi de Conques (2017SGR-596) are also acknowledged for their financial support. Part of the presented models have been carried out at the Geomodels Analogue Modelling Laboratory, a Scientific Infrastructure grant (UNBA08-4E-006) co-funded by the European Regional Development Fund of the Ministerio de Ciencia e Innovación of the Spanish Government and Statoil (currently Equinor). Finally, we thank T. Dooley for providing original figures that we modified, R. Butler and T. Dooley for helpful reviews, C. Luneburg for inviting this contribution to the Special Issue honoring John Ramsay, and of course John himself for his immense contributions to the field and his ongoing inspiration to all of us.

References

- Bonini, M., 2003. Detachment folding, fold amplification, and diapirism in thrust wedge experiments. *Tectonics* 22. <https://doi.org/10.1029/2002TC001458>.
- Borderie, S., Graveleau, F., Witt, C., Vendeville, B.C., 2018. Impact of interbedded viscous décollement on the structural and kinematic coupling in fold-and-thrust belts: insights from analogue modeling. *Tectonophysics*. 722, 118-137. <http://dx.doi.org/10.1016/j.tecto.2017.10.019>.
- Brun, J.-P., Fort, X., 2004. Compressional salt tectonics (Angolan margin). *Tectonophysics*. 382, 129-150. <http://dx.doi.org/10.1016/j.tecto.2003.11.014>.
- Brun, J.-P., Mauduit, T.P.-O., 2008. Rollovers in salt tectonics: the inadequacy of the listric fault model. *Tectonophysics*. 457, 1-11. <https://doi.org/10.1016/j.tecto.2007.11.038>.
- Butler, R.W.H., Bond, C.E., Cooper, M.A., 2020. Henry Cadell's 'Experimental researches in mountain building': their lessons for interpreting thrust systems and fold-thrust systems. In: Hammerstein, J.A., Di Cuia, R., Cottam, M.A., Zamora, G., Butler, R.W.H. (Eds.), *Fold and Thrust Belts: Structural Style, Evolution and Exploration*: Geol. Soc. London Spec. Pub. 490. <https://doi.org/10.1144/SP490-2019-142>.
- Callot, J.-P., Jahani, S., Letouzey, J., 2007. The role of pre-existing diapirs in fold and thrust belt development. In: Lacombe, O., Lavé, J., Roure, F.M., Vergés, J. (Eds.), *Thrust Belts and Foreland Basins*. Springer, Berlin, 307-323. http://dx.doi.org/10.1007/978-3-540-69426-7_16.
- Callot, J.-P., Trocmé, V., Letouzey, J., Albouy, E., Jahani, S., Sherkati, S., 2012. Pre-existing salt structures and the folding of the Zagros Mountains. In: Alsop, G.I., Archer, S.G., Hartley, A.J., Grant, N.T., Hodgkinson, R. (Eds.), *Salt Tectonics, Sediments and Prospectivity*. Geol. Soc. Spec. Pub. 363, 545-561. <http://dx.doi.org/10.1144/SP363.27>.
- Cámara, P., 2017. Salt and strike-slip tectonics as main drivers in the structural evolution of the Basque-Cantabrian Basin, Spain. In: Soto, J.I., Flinch, J.F., Tari, G. (Eds.), *Permo-Triassic salt provinces of Europe, North Africa and the Atlantic margins*. Elsevier, Amsterdam, 371-393. <http://dx.doi.org/10.1016/B978-0-12-809417-4.00018-5>.
- Célini, N., Callot, J.-P., Ringenbach, J.-C., Graham, R., 2020. Jurassic salt tectonics in the SW Sub-Alpine fold-and-thrust belt. *Tectonics* 39. <https://doi.org/10.1029/2020TC006107>.
- Costa, E., Vendeville, B.C., 2002. Experimental insights on the geometry and kinematics of fold-and-thrust belts above weak, viscous evaporitic décollement. *J. Struct. Geol.* 24, 1729-1739. [http://dx.doi.org/10.1016/S0191-8141\(01\)00169-9](http://dx.doi.org/10.1016/S0191-8141(01)00169-9).
- Coward, M.P., Stewart, S., 1995. Salt-influenced structures in the Mesozoic-Tertiary cover of the southern North Sea, U.K. In: Jackson, M.P.A., Roberts, D. G., Snelson, S., (Eds.), *Salt Tectonics: a Global Perspective*. AAPG Memoir 65, 229-250. <https://doi.org/10.1306/M65604C10>.
- Davis, D.M., Engelder, T., 1985. The role of salt in fold-and-thrust belts. *Tectonophysics*. 119, 67-88. [https://doi.org/10.1016/0040-1951\(85\)90033-2](https://doi.org/10.1016/0040-1951(85)90033-2).
- Davison, I., 2020. Salt tectonics in the Sureste Basin, SE Mexico: some implications for hydrocarbon exploration. In: Davison, I., Hull, J.N.F., Pindell, J. (Eds.), *The Basins, Orogens and Evolution of the Southern Gulf of Mexico and Northern Caribbean*. Geol. Soc., London, Spec. Pub. 504. <https://doi.org/10.1144/SP504-2019-227>.
- Dooley, T.P., Hudec, M.R., 2020. Extension and inversion of salt-bearing rift systems. *Solid Earth* 11, 1187-1204. <https://doi.org/10.5194/se-11-1187-2020>.

- Dooley, T.P., Jackson, M.P.A., Hudec, M.R., 2009a. Deformation styles and linkage of salt walls during oblique shortening. AAPG Search and Discovery Article #90090©2009. <https://www.searchanddiscovery.com/abstracts/html/2009/annual/abstracts/dooley.htm>.
- Dooley, T.P., Jackson, M.P.A., Hudec, M.R., 2009b. Inflation and deflation of deeply buried salt stocks during lateral shortening. *J. Struct. Geol.* 31, 582-600. <https://doi.org/10.1016/j.jsg.2009.03.013>.
- Dooley, T.P., Jackson, M.P.A., Hudec, M.R., 2015. Breakout of squeezed stocks: dispersal of roof fragments, source of extrusive salt and interaction with regional thrust faults. *Bas. Res.* 27, 3-25. <https://doi.org/10.1111/bre.12056>.
- Duffy, O.B., Dooley, T.P., Hudec, M.R., Jackson, M.P.A., Fernandez, N., Jackson, C.A.-L., Soto, J.I., 2018. Structural evolution of salt-influenced fold-and-thrust belts: a synthesis and new insights from basins containing isolated salt diapirs. *J. Struct. Geol.* 114, 206-221. <https://doi.org/10.1016/j.jsg.2018.06.024>
- Duffy, O.B., Fernandez, N., Hudec, M.R., Jackson, M.P.A., Burg, G., Dooley, T.P., Jackson, C.A.-L., 2017. Lateral mobility of minibasins during shortening: insights from the SE Precaspian Basin, Kazakhstan. *J. Struct. Geol.* 97, 257-276. <http://dx.doi.org/10.1016/j.jsg.2017.02.002>.
- Ferrer, J.O., 2012. Salt Tectonics in the Parentis Basin (Eastern Bay of Biscay): Origin and Kinematics of Salt Structures in a Hyperextended Margin Affected by Subsequent Contractual Deformation: Ph.D. thesis, Univ. of Barcelona.
- Giles, K.A., Lawton, T.F., 2002. Halokinetic sequence stratigraphy adjacent to the El Papalote diapir, northeastern Mexico. *AAPG Bull.* 86, 823-840. <https://doi.org/10.1306/61EEDBAC-173E-11D7-8645000102C1865D>.
- Giles, K.A., Rowan, M.G., 2012. Concepts in halokinetic-sequence deformation and stratigraphy. In: Alsop, G.I., Archer, S.G., Hartley, A.J., Grant, N.T., Hodgkinson, R. (Eds.), *Salt Tectonics, Sediments and Prospectivity*. *Geol. Soc. Spec. Pub.* 363, 7-31. <https://doi.org/10.1144/SP363.2>.
- Gottschalk, R.R., Anderson, A.V., Walker, J.D., Da Silva, J.C., 2004. Modes of contractional salt tectonics in Angola Block 33, Lower Congo Basin, West Africa. In: Post, P.J., Olson, D.L., Lyons, K.T., Palmes, S.L., Harrison, P.F., Rosen, N.C. (Eds.), *Salt-Sediment Interactions and Hydrocarbon Prospectivity: Concepts, Applications, and Case Studies for the 21st Century*. 24th Annual GCSSEPM Foundation Bob F. Perkins Research Conference, 220-242. <https://doi.org/10.5724/gcs.04.24.0705>.
- Granado, P., Roca, E., Strauss, P., Pelz, K., Muñoz, J.A., 2018. Structural styles in fold-and-thrust belts involving early salt structures: the Northern Calcareous Alps (Austria). *Geology*. <https://doi.org/10.1130/G45281.1>.
- Grando, G., McClay, K., 2004. Structural evolution of the Frampton growth fold system, Atwater Valley - southern Green Canyon area, deep water Gulf of Mexico. *Mar. Pet. Geol.* 21, 889-910. <https://doi.org/10.1016/j.marpetgeo.2003.12.005>.
- Guglielmo, G. Jr., Vendeville, B.C., Jackson, M.P.A., 2000. 3-D visualization and isochore analysis of extensional diapirs overprinted by compression. *AAPG Bull.* 84, 1095-1108. <https://doi.org/10.1306/A9673C48-1738-11D7-8645000102C1865D>.
- Hassanpour, J., Jahani, S., Ghassemi, M.R., Alavi, S.A., Zeinali, F., 2018. Evolution of the Karebas Fault system and adjacent folds, central Zagros fold-and-thrust belt, Iran: role of pre-existing halokinesis (salt structures and minibasins) and detachment levels. *J. Asian Ear. Sci.* 164, 125-142. <https://doi.org/10.1016/j.jseae.2018.06.024>.

- Hearon, T.E. IV, Rowan, M.G., Giles, Hart, W.H., 2014. Halokinetic deformation adjacent to the deepwater Auger diapir, Garden Banks 470, northern Gulf of Mexico: testing the applicability of an outcrop-based model using subsurface data. *Interpretation* 2, SM57-SM76. <https://doi.org/10.1190/INT-2014-0053.1>.
- Hudec, M.R., Jackson, M.P.A., 2006. Advance of allochthonous salt sheets in passive margins and orogens. *AAPG Bull.* 90, 1535-1564. <https://doi.org/10.1306/05080605143>.
- Hudec, M.R., Jackson, M.P.A., Peel, F.J., 2013. Influence of deep Louann structure on the evolution of the northern Gulf of Mexico. *AAPG Bull.* 97, 1711-1735. <https://doi.org/10.1306/04011312073>.
- Jackson, M.P.A., Hudec, M.R., Jennette, D.C., Kilby, R.C., 2008. Evolution of the Cretaceous Astrid thrust belt in the ultradeep-water Lower Congo Basin, Gabon. *AAPG Bull.* 92, 487-511. <https://doi.org/10.1306/12030707074>.
- Jahani, S., Callot, J.-P., Letouzey, J., Frizon de Lamotte, D., 2009. The eastern termination of the Zagros fold-and-thrust belt, Iran: structures, evolution, and relationships between salt plugs, folding, and faulting. *Tectonics* 28. <https://doi.org/10.1029/2008TC002418>.
- Karlo, J.F., van Buchen, F.S.P., Moen, J., Milroy, K., 2014. Triassic-age salt tectonics of the Central North Sea. *Interpretation* 2, SM19-SM28. <https://doi.org/10.1190/INT-2014-0032.1>.
- Koyi, H., 1998. The shaping of salt diapirs. *J. Struct. Geol.* 20, 321-338. [https://doi.org/10.1016/S0191-8141\(97\)00092-8](https://doi.org/10.1016/S0191-8141(97)00092-8).
- Letouzey, J., Colletta, B., Vially, R., Chermette, J.C., 1995. Evolution of salt-related structures in compressional settings. In: Jackson, M.P.A., Roberts, D. G., Snelson, S., (Eds.), *Salt Tectonics: a Global Perspective*. AAPG Memoir 65, 41-60. <https://doi.org/10.1306/M65604C3>.
- Letouzey, J., Sherkati, S., 2004. Salt movement, tectonic events, and structural style in the central Zagros fold and thrust belt (Iran). In: Post, P.J, Olson, D.L., Lyons, K.T., Palmes, S.L., Harrison, P.F., Rosen, N.C. (Eds.), *Salt-Sediment Interactions and Hydrocarbon Prospectivity: Concepts, Applications, and Case Studies for the 21st Century*. 24th Annual GCSSEPM Foundation Bob F. Perkins Research Conference, 220-242. <https://doi.org/10.5724/gcs.04.24.0753>.
- Mount, V.S., Dull, K., Mentemeier, S., 2007. Structural style and evolution of traps in the Paleogene play, deepwater Gulf of Mexico. In: Kennan, L., Pindell, J., Rosen, N.C. (Eds.), *The Paleogene of the Gulf of Mexico and Caribbean Basins*. 27th Annual GCSSEPM Foundation Bob F. Perkins Research Conference, CD-ROM. <https://doi.org/10.5724/gcs.07.27.0054>.
- Nilsen, K.T., Vendeville, B.C., Johansen, J.-T., 1995. Influence of regional tectonics on halokinesis in the Nordkapp Basin, Barents Sea. In: Jackson, M.P.A., Roberts, D. G., Snelson, S., (Eds.), *Salt Tectonics: a Global Perspective*. AAPG Memoir 65, 413-436. <https://doi.org/10.1306/M65604C20>.
- Parravano, V., Teixell, A., Mora, A., 2015. Influence of salt in the tectonic development of the frontal thrust belt of the eastern Cordillera (Guatiquía area, Colombian Andes). *Interpretation* 3, 17-27. <https://doi.org/10.1190/INT-2015-0011.1>.
- Pichel, L.M., Jackson, C.A.-L., 2020. Four-dimensional variability of composite halokinetic sequences. *Bas. Res.* 32, 1277-1299. <https://doi.org/10.1111/bre.12428>.
- Pla, O., Roca, E., Xie, H., Izquierdo-Llavall, E., Muñoz, J.A., Rowan, M.G., Ferrer, O., Gratacós, O., Yuan, N., Huang, S., 2019. Influence of syntectonic sedimentation and

- décollement rheology on the geometry and evolution of orogenic wedges: analog modeling of the Kuqa fold-and-thrust belt (NW China). *Tectonics*. <https://doi.org/10.1029/2018TC005386>.
- Roca, E., Sans, M., Koyi, H.A., 2006. Polyphase deformation of diapiric areas in models and in the eastern Prebetics (Spain). *AAPG Bull.* 90, 115-136. <https://doi.org/10.1306/07260504096>.
- Roma, M., Ferrer, O., McClay, K.R., Muñoz, J.A., Roca, E., Gratacós, O., Cabello, P., 2018. Weld kinematics of synrift salt during basement-involved extension and subsequent inversion: results from analog models. *Geol. Acta.* 16, 391-410. <https://doi.org/10.1344/GeologicaActa2018.16.4.4>.
- Rowan, M.G., 2019. Gravity-driven and tectonic deformation in the southern Gulf of Mexico – extended abstract. Conference Proceedings, Second EAGE Workshop on Deepwater Exploration in Mexico, Cancun, Mexico. <https://doi.org/10.3997/2214-4609.201900360>.
- Rowan, M.G., 2020. Salt- and shale-detached gravity-driven failure of continental margins. In: Scarselli, N., Adam, J., Chiarella, D., Roberts, D.G., Bally, A.W. (Eds.), *Regional Geology and Tectonics, Vol. 1: Principles of Geologic Analysis*, 2nd Ed. Elsevier, Amsterdam, 205-234. <https://doi.org/10.1016/B978-0-444-64134-2.00010-9>.
- Rowan, M.G., Giles, K.A., 2022. Different scales of salt-sediment interaction flanking passive diapirs. *AAPG Bull.*, in press.
- Rowan, M.G., Giles, K.A., Hearon, T.E. IV, Fiduk, J.C., 2016. Megaflaps adjacent to salt diapirs. *AAPG Bull.* 100, 1723-1747. <https://doi.org/10.1306/05241616009>.
- Rowan, M.G., Lawton, T.F., Giles, K.A., Ratliff, R.A., 2003. Near-salt deformation in La Popa basin, Mexico, and the northern Gulf of Mexico: a general model for passive diapirism. *AAPG Bull.* 87, 733-756. <https://doi.org/10.1306/01150302012>.
- Rowan, M.G., Peel, F.J., Vendeville, B.C., 2004. Gravity-driven foldbelts on passive margins. In: McClay, K.R. (Ed.), *Thrust Tectonics and Hydrocarbon Systems*. *AAPG Mem.* 82, 157-182. <https://doi.org/10.1306/M82813C9>.
- Rowan, M.G., Ratliff, R.A., 2012. Cross-section restoration of salt-related deformation: best practices and potential pitfalls. *J. Struct. Geol.* 41, 24-37. <https://doi.org/10.1016/j.jsg.2011.12.012>.
- Rowan, M.G., Trudgill, B.D., Fiduk, J.C., 2000. Deep-water, salt-cored foldbelts: lessons from the Mississippi Fan and Perdido foldbelts, northern Gulf of Mexico. In: Mohriak, W., Talwani, M. (Eds.), *Atlantic Rifts and Continental Margins*. *AGU Geophys. Monograph* 115, 173-191. <https://doi.org/10.1029/GM115p0173>.
- Rowan, M.G., Vendeville, B.C., 2006. Foldbelts with early salt withdrawal and diapirism: physical model and examples from the northern Gulf of Mexico and the Flinders Ranges, Australia. *Mar. Pet. Geol.* 26, 871-891. <https://doi.org/10.1016/j.marpetgeo.2006.08.003>.
- Sánchez Rivera, R., Cruz Mercado, M.Á., Reyes Tovar, E., López Céspedes, H.G., Peterson Rodríguez, R.H., Flores Zamora, J.C., León Ramirez, R., Barrera González, D., 2011. Tectonic evolution of the South Gulf Salt Province in the Gulf of Mexico. *Gulf Coast Assoc. Geol. Soc. Trans.* 61, 421-427.
- Sans, M., Koyi, H.A., 2001. Modeling the role of erosion in diapir development in contractional settings. In: Koyi, H.A., Mancktelow, N.S. (Eds.), *Tectonic Modeling: a Volume in Honor of Hans Ramberg*. *GSA Mem.* 193, 111-122. <https://doi.org/10.1130/0-8137-1193-2.111>.
- Santolaria, P., Ferrer, O., Rowan, M.G., Snidero, M., Carrera, N., Granado, P., Muñoz, J.A., Roca, E., Schneider, C., Piña, A., Zamora, G., 2021a. Influence of preexisting salt diapirs during thrust wedge evolution and secondary welding: insights from analog modeling. *J. Struct. Geol.* 149. <https://doi.org/10.1016/j.jsg.2021.104374>.

- Santolaria, P., Granado, P., Carrera, P., Schneider, C., Ferrer, O., Snidero, M., Strauss, P., Pelz, K., Roca, E., Muñoz, J.A., 2021b. From downbuilding to contractional restoration of salt-sediment systems: insights from analog modeling. *Tectonophys.* 819. <https://doi.org/10.1016/j.tecto.2021.229078>.
- Santolaria, P., Vendeville, B.C., Graveleau, F., Soto, R., Casas-Sainz, A., 2015. Double evaporitic décollements: influence of pinch-out overlapping in experimental thrust wedges. *J. Struct. Geol.* 76, 35-51. <http://dx.doi.org/10.1016/j.jsg.2015.04.002>.
- Saura, E., Vergés, J., Martín-Martín, J.D., Messenger, G., Moragas, M., Razin, P., Grélaud, C., Joussiaume, R., Malaval, M., Homke, S., Hunt, D.W., 2014. Syn- to post-rift diapirism and minibasins of the Central High Atlas (Morocco): the changing face of a mountain belt. *J. Geol. Soc.* 171, 97-105. <https://doi.org/10.1144/jgs2013-079>.
- Sebai, N., Vendeville, B.C., Boukadi, N., Dhahri, F., 2021. The perched synclines look-alike of central Tunisia: examples of diapir rise–fall–rise illustrated by field, geophysical and experimental data. *J. Struct. Geol.* 147. <https://doi.org/10.1016/j.jsg.2021.104336>.
- Smit, J.H.W., Brun, J.P., Sokoutis, D., 2003. Deformation of brittle-ductile thrust wedges in experiments and nature. *J. Geophys. Res.* 108. <https://doi.org/10.1029/2002JB002190>.
- Snidero, M., Muñoz, J.A., Carrera, N., Butillé, M., Mencos, J., Motamedi, H., Piryaei, A., Sàbat, F., 2019. Temporal evolution of the Darmadan salt diapir, eastern Fars region, Iran. *Tectonophys.* 766, 115-130. <https://doi.org/10.1016/j.tecto.2019.06.006>.
- Talbot, C. J., Alavi, M., 1996. The past of a future syntaxis across the Zagros. *Geol. Soc., London, Spec. Pub.* 100, 89-109. <https://doi.org/10.1144/GSL.SP.1996.100.01.08>.
- Tămaș, D.M., Tămaș, A., Barabasch, J., Rowan, M.G., Schleder, Z., Krézsek, C., Urai, J.L., 2021. Low-angle shear within the exposed Mânzălești Diapir, Romania: salt decapitation in the eastern Carpathians fold-and-thrust belt. *Tectonics* 40. <https://doi.org/10.1029/2021TC006850>.
- Vendeville, B.C., Jackson, M.P.A., 1992. The rise of diapirs during thin-skinned extension. *Mar. Pet. Geol.* 9, 331-353. [https://doi.org/10.1016/0264-8172\(92\)90047-I](https://doi.org/10.1016/0264-8172(92)90047-I).
- Vendeville, B.C., Nilsen, K.T., 1995. Episodic growth of salt diapirs driven by horizontal shortening. In: Travis, C.J., Harrison, H., Hudec, M.R., Vendeville, B.C., Peel, F.J., Perkins, B.F. (Eds.), *Salt, Sediment, and Hydrocarbons: 16th Annual GCSSEPM Foundation Bob F. Perkins Res. Conf.*, 285-295. <https://doi.org/10.5724/gcs.95.16.0285>.
- Vidal-Royo, O., Rowan, M.G., Ferrer, O., Fischer, M.P., Fiduk, J.C., Canova, D.P., Hearon, T.E. IV, Giles, K.A., 2021. The transition from salt diapir to weld and thrust: examples from the Northern Flinders Ranges in South Australia. *Bas. Res.* <https://doi.org/10.1111/bre.12579>.

Supplementary Material

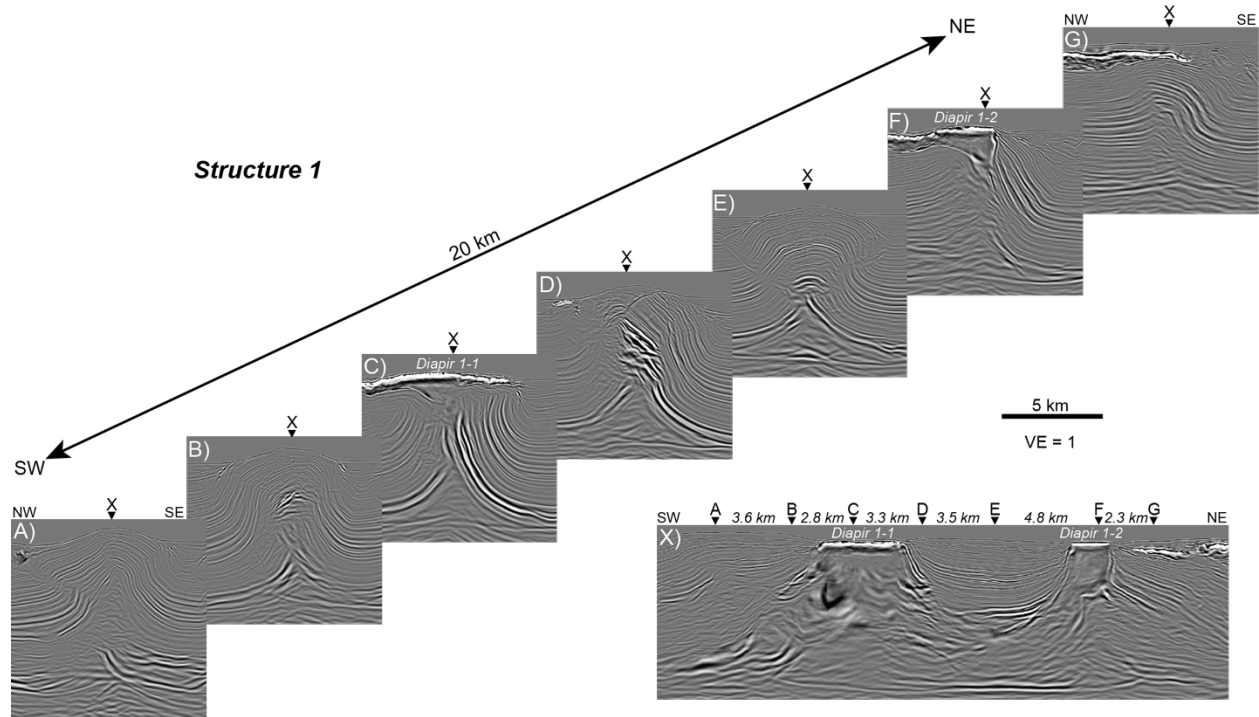


Fig. S1. Uninterpreted versions of depth-migrated seismic profiles of Fig. 3 (WAZ RTM data courtesy of Schlumberger).

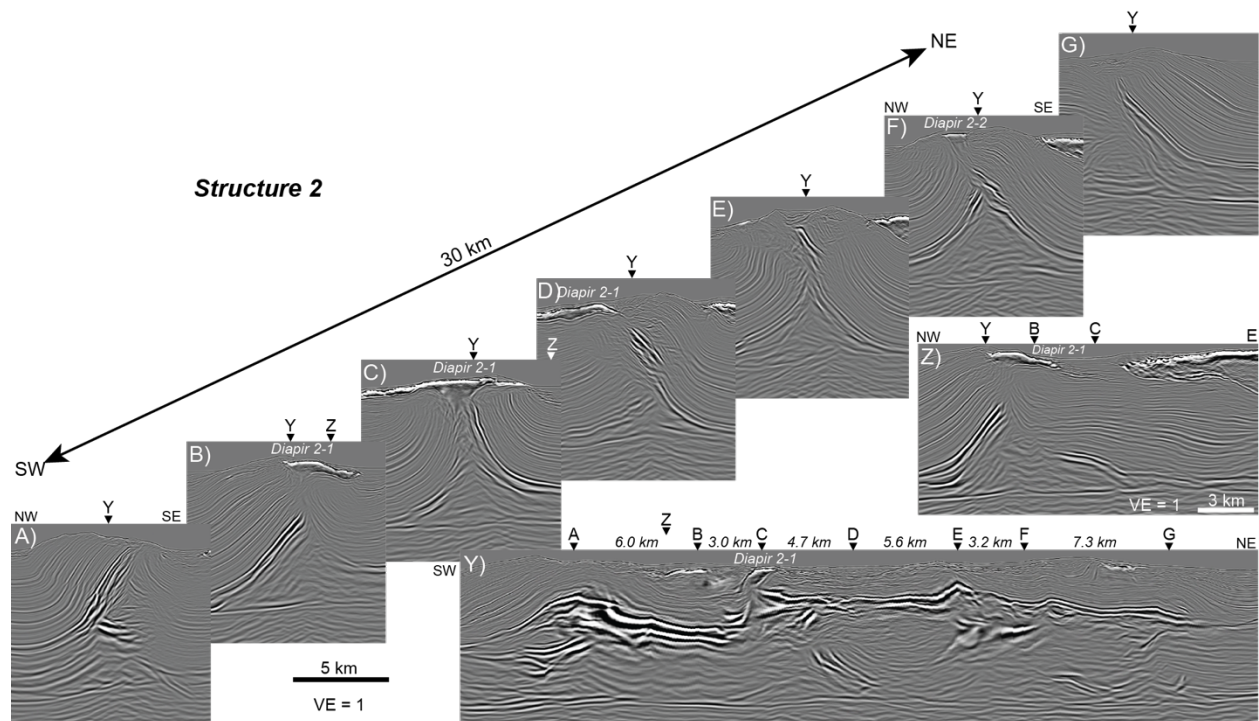


Fig. S2. Uninterpreted versions of depth-migrated seismic profiles of Fig. 5 (WAZ RTM data courtesy of Schlumberger).